A New Entry to Purely Organic Thermally Activated Delayed Fluorescence Emitters Based on Pyrido[2,3-**b**]pyrazine–Dihydrophenazasilines Donor–Acceptor Dyad

Goya, Tsuyoshi; Crocomo, Paola Zimmermann; Hosono, Takumi; Minakata, Satoshi; de Sousa, Leonardo Evaristo; de Silva, Piotr; Data, Przemyslaw; Takeda, Youhei

Published in:
Asian Journal of Organic Chemistry

Link to article, DOI:
10.1002/ajoc.202100780

Publication date:
2022

Document Version
Publisher's PDF, also known as Version of record

ACES Asian Chemical Editorial Society

doi.org/10.1002/ajoc.202100780

ASIAN JOURNAL OF ORGANIC CHEMISTRY
Research Article

www.asianjoc.org

Special Collection

A New Entry to Purely Organic Thermally Activated Delayed Fluorescence Emitters Based on Pyrido[2,3-*b*]pyrazine-Dihydrophenazasilines Donor-Acceptor Dyad

Tsuyoshi Goya[+],[a] Paola Zimmermann Crocomo[+],[b] Takumi Hosono,[c] Satoshi Minakata,[c] Leonardo Evaristo de Sousa,[d] Piotr de Silva,*[d] Przemyslaw Data,*[b] and Youhei Takeda*[c]

Abstract: A new family of thermally activated delayed fluorescence (TADF) emitters based on a twisted donor-acceptor (D–A) dyad scaffold comprising of dihydrophenazasiline (D) and pyrido[2,3-*b*]pyrazine (A) has been developed, and their properties have been investigated. Time-resolved spectroscopic analysis in matrices revealed the detailed photophysical properties of the D–A compounds. These D–A compounds serve as the emitter for organic light-emitting diodes (OLEDs), showing a moderate external quantum efficiency (EQE) up to 9% in CBP matrix. Furthermore, theoretical calculations uncovered the excited states nature of the developed TADF emitters.

Introduction

Over the last decade, organic compounds that can display thermally activated delayed fluorescence (TADF) have rapidly attracted much attention as the emitter for efficient organic light-emitting diodes (OLEDs), as they can harvest electrically generated triplet excitons and convert into the emissive singlet excitons through reverse intersystem crossing (rISC) to achieve theoretically 100% internal quantum efficiency (IQE).[1,2] In addition to OLEDs, the high capability of harvesting triplet excited states allows for diverse applications of TADF-active organic compounds, spanning from time-resolved bio-imaging[3–5] to organic photoredox catalysis.[6] Therefore, the development of new TADF organic compounds and investigation of their photophysical properties contributes to the further understanding of underlying principles and the advancement of materials science.

As our reseach program on the development of organic materials, we have developed a variety of photofunctional organic compounds based on a dibenzo[*a,j*]phenazine (DBPHZ)-cored donor-acceptor-donor (D–A–D) or donor-acceptor-donor-acceptor (D–A–D–A) scaffold,[7] which are featured with efficient TADF,[8,9] room-temperature phosphorescence (RTP),[10] TADF/RTP-active mechanochromism,[11,12] and hydrochromism,[13] for instance. A significant finding through the structure-relationship studies of the series of D–A type compounds includes that the photophysics of the D–A–D compounds are highly affected by the donor conformation and bridging heteroatoms on the donor units. Based on this findings, we decided to explore a new D–A system that can show TADF, by applying a much simpler system. We focused on the use of electron-deficient azaaromatic scaffold in place of DBPHZ unit. Pyrido[2,3-*b*]pyrazine (PYPZ) unit was selected as the electron-acceptor (A), as the skeleton has multiple sp^2-hybrized nitrogen atoms in the π conjugated backbone and thereby guarantees the high electron-affinity. Also, the PYPZ family is readily prepared through a simple condensation protocol between 2,3-diaminopyridines and benzil derivatives. Owing to the multiple embedded N(sp^2) atoms in the naphthalene skeleton, the T_1 state of PYPZ is ^{3}(n,π*) state.[14] Therefore, if this electron-deficient core is connected with an appropriate electron-donor (D), intramolecular charge-transfer (ICT) in the exited state would occur and the CT states should become the first singlet excited state (S_1). Additionally, mixing of the intrinsic ^{3}(n,π*) nature of the electron-acceptor core and CT/π,π* excied states would allow for relaxing the El-Sayed rule[15] by increasing the spin-orbit coupling (SOC) between the excited singlet and triplet states. As for donor pat, we selected dihydrophenazasiline (DHPAzSi), as DHPAzSi compounds serve as a moderate electron donor, due to the operation of σ*(C–Si)-π hyperconjugation, thereby allowing for the ^{1}CT state in proximity to a

[a] *T. Goya[+]*
New Business Commercialization Project
NIPPON SHOKUBAI CO., LTD.
5-8 Nishi Otabi-cho, Suita, Osaka 564-0034 (Japan)

[b] *P. Zimmermann Crocomo,[+] Prof. Dr. P. Data*
Faculty of Chemistry
Silesian University of Technology
M. Strzody 9, 44-100, Gliwice (Poland)
E-mail: przemyslaw.data@polsl.pl

[c] *T. Hosono, Prof. Dr. S. Minakata, Prof. Dr. Y. Takeda*
Department of Applied Chemistry
Graduate School of Engineering
Osaka University
Yamadaoka 2–1, Suita, Osaka 565-0871 (Japan)
E-mail: takeda@chem.eng.osaka-u.ac.jp

[d] *Dr. L. E. de Sousa, Prof. Dr. P. de Silva*
Department of Energy Conversion and Storage
Technical University of Denmark
2800 Kongens Lyngby (Denmark)
E-mail: pdes@dtu.dk

[+] *These authors contributed equally to this work.*

Supporting information for this article is available on the WWW under https://doi.org/10.1002/ajoc.202100780

This manuscript is part of a special collection celebrating the 10th Anniversary of the Asian Journal of Organic Chemistry.

higher triplex excited state (T_n) to undergo (reverse) intersystem crossing via T_n state.[10] Although D–A type organic photofunctional materials containing the pyrido[2,3-*b*]pyrazine as the acceptor have recently been developed by several groups,[16–20] TADF emitters based on the pyrido[2,3-*b*]pyrazine-acceptor and dihydrophenazasiline donor have been unknown. Herein, we disclose the synthesis and photophysical properties of a new family of D–A type purely organic TADF emitters **1**–**3** (Figure 1), using the dihydrophenazasiline as the donor and pyrido[2,3-*b*]pyrazine as the acceptor.

Results and Discussion

Materials Synthesis

The synthetic routes to **1**–**3** are shown in Scheme 1. The 7-bromo-2,3-diphenylpyrido[2,3-*b*]pyrazine (**4**) and 10-bromo-acenaphtho[1,2-*b*]pyrido[2,3-*e*]pyrazine (**6**) were easily prepared through the condensation between 2,3-diamino-5-bromopyradine with benzil and phenanthrene-9,10-dione, respectively, according to the procedures in literature.[21,22] D–A compounds **1**–**3** were synthesized in good yields through the Pd-catalyzed Buchwald-Hartwig amination of **4**/**6** with the corresponding DHPAzSi derivative (Scheme 1, and the detailed procedures and the spectroscopic data of the products are described in the Supporting Information).

Time-Resolved Spectroscopic Analysis

To investigate the photophysical properties of compounds **1**–**3**, time-resolved luminescence spectroscopic analysis was conducted in a non-polar polymer matrix Zeonex® (Figure 2), and in small molecule hosts, 4,4′-bis(*N*-carbazolyl)-1,1′-biphenyl (CBP)

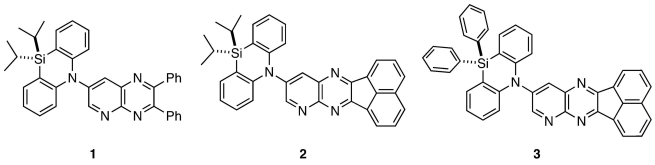

Figure 1. The chemical structures of investigated materials.

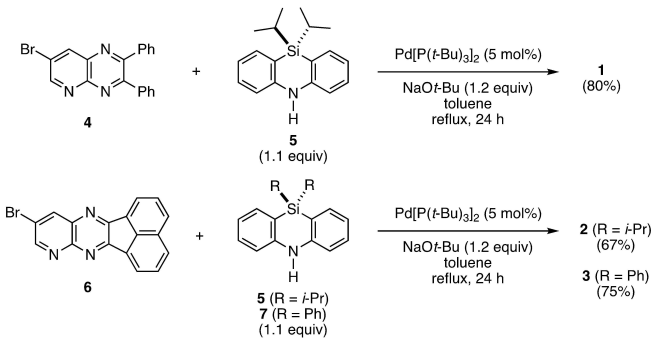

Scheme 1. Synthesis of D–A compounds **1**–**3**.

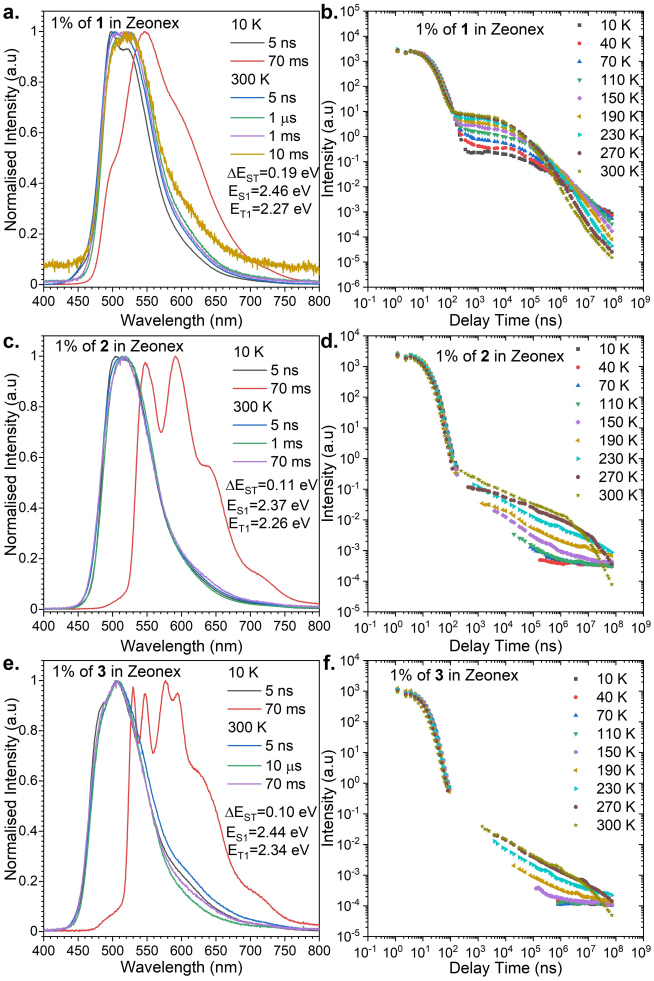

Figure 2. Time-resolved PL spectra and photoluminescence decay profiles (intensity vs. delay time) of **1**–**3** in Zeonex® matrix. The energies are estimated from to the maximum emission peaks.

(Figure S4) and tris(4-(9*H*-carbazoyl-9-yl)phenyl)amine (TCTA) (Figure S5). In all of the cases, compounds **1**–**3** exhibited emissions in two distinct time regions (Figure 2b, d, and f). The first component, decaying with a lifetime in the nanosecond time delay is the prompt fluorescence (PF) from the singlet excited state (S_1), and the second components decaying in micro to millisecond delay time are the delayed emissions (Figure 2, S4, and S5). When we look at the spectra more closely, all three compounds display more resolved prompt emission in Zeonex® matrix than in CBP and TCTA, and the emission spectra in CBP and TCTA are broader and at the longer wavelength region, when compared with in Zeonex® matrix. This phenomenon should be caused by the change in nature of the lowest singlet excited state: in non-polar matrix (Zeonex®), the observed emission is radiated from the locally excited state (^{1}LE) (Figure 2a, c, and e), while in CBP and TCTA hosts, the emission comes from charge-transfer excited state (^{1}CT) (Figure S4a, c, e, Figure S5a, c, and e).

Depending on the experimental temperature, we observed the change in spectra and emission intensity in the micro-second time delay, whereas the prompt emission appeared to

be unchanged. The reason why such phenomenon was observed would be that delay emission is mainly contributed from the triplet excited states. At low temperature (10 K) and millisecond time delay, the phosphorescence was observed (spectra in red), and emission intensity decreased with the rise of temperature. On the other hand, the triplet excited states are transferred to the singlet excited states, due to the thermal activation of reverse intersystem crossing (rISC) causing TADF emission with the rise of temperature (Figure 2). In all the cases, at room temperature, only delayed emission through TADF mechanism was observed. Specifically, the TADF emission is very intense in Zeonex® matrix with a DF/PF ratio above 3 (Table 1), which correspond to almost 100% of recycling triplet excited state. When we look closely to the transient decays, the compound **1** exhibits the fastest decay profile (lower amount of ISC/rISC cycling) which together with high DF/PF ratio resulted high triplet conversion and TADF contribution. The fusion of the adjacent two phenyl units (compound **2**) enlarges the overall π-conjugation, which resulted in a slight decrease in singlet and triplet energy when compared to compound **1** (Figure 2). Also, the expansion of π-conjugation (compound **2**) drastically decreases the overall photoluminescence quantum yield (Table 1). When the isopropyl groups on the Si center of the donor were replaced with phenyl groups (compound **3**), additional decrease of efficiency and delayed fluorescence intensity was observed (Figure 2 and Table 1). This was mostly attributed to the steric hindrance to restrict the oscillation between the donor and acceptor moieties and thereby decrease the efficiency of intramolecualr charge transfer process. The photoluminescence spectra were shifted to the lower energy region in CBP and TCTA matrix, which allows for stabilizing the ^{1}CT state by more polar nature, when compared with Zeonex®. Although the ^{1}CT state is stabilized, the single-triplet energy gap ΔE_{ST} appeared to be independent from CT state energy, which may be the variation in the triplet excited state (T_1) energy (Table 1). Intriguingly, the rISC process decreased, and the DF/PF ratio dropped more than half of values in Zeonex® (Table 1).

OLEDs Fabrication and Characterization

To fabricate the OLEDs using the materials **1**–**3**, the thermal stability of the compounds was investigated by the thermogravimetric analysis (TGA, Figure S1 and S2). All the compounds have a high degradation temperature T_d (5 wt% loss under N_2 gas) above 300 °C in the order of **3** (405 °C) > **2** (359 °C) > **1** (338 °C), which is consistent with the number of aromatic rings included in molecule and molecular rigidity. These values implied the feasibility of the fabrication of OLED devices through vacuum thermal evaporation (VTE) technique. Furthermore, the investigation of the glass transition temperature (T_g) of emitters **1**–**3** with differential scanning calorimetry (DSC) revealed the relatively high T_g [**1**: 92 °C, **2**: 110 °C, **3**: 113 °C] (Figure S3), which allow for morphological stability in OLED devices. The T_g values are comparable with those of similar PYPZ-based D–A compounds.[18]

To evaluate the possible use of emitters in OLED structure, the electrochemical analysis was conducted. All compounds exhibited a reversible reduction and an irreversible oxidation process (Figure S6). The estimated ionization potential (IP)/electron affinity (EA) of **1**–**3** determined with the CV experiments are 5.78 eV/3.35 eV, 5.79 eV/3.44 eV, 5.88 eV/3.47 eV, respectively (Figure S6). Compounds **1** and **2** share the same donor, and the IP energy values are similar. Also, a similar situation for the EA values of compounds **2** and **3** applies, where they share the same acceptor unit. These facts imply that the D–A systems in all the compounds are highly twisted and the HOMO and LUMO is distinctly separated to allow for small ΔE_{ST} values.

To evaluate the possibility of the use of the developed compounds as TADF-OLED emitters, devices were fabricated through co-evaporation technique (for the details, see the Supporting Information). The fabricated device structures are as follows: Devices 1–3 ITO/NPB [*N*,*N*′-di(1-naphthyl)-*N*,*N*′-diphenyl-(1,1′-biphenyl)-4,4′-diamine] (40 nm)/TSBPA [4,4′-(diphenylsilanediyl)bis(*N*,*N*-diphenylaniline)] (10 nm)/10% **1**, **2** or **3** in CBP (30 nm)/TPBi [2,2′,2″-(1,3,5-benzinetriyl)-tris(1-phenyl-1-*H*-benzimidazole)] (50 nm)/LiF (1 nm)/Al (100 nm); Devices 4–6 ITO/NPB (40 nm)/TAPC [4,4′-cyclohexylidenebis(*N*,*N*-bis(4-methylphenyl)benzenamine)] (10 nm)/10% **1**, **2** or **3** in TCTA (30 nm)/TPBi [2,2′,2″-(1,3,5-benzinetriyl)-tris(1-phenyl-1-*H*-

Table 1. Summary of the general photophysical properties of **1**–**3**.

Compound	Host	λ_{em} [nm][a]	Φ_{PL}[b]	τ_{PF} [ns][c]	τ_{DF} [μs][d]	DF/PF[e]	E_a [eV][f]	S_1 [eV][g]	T_1 [eV][g]	ΔE_{ST} [eV][h]
1	Zeonex®	527	0.25	13.24 ± 1.18	9.45 ± 0.98	6.08	0.024	2.46	2.27	0.19
	CBP	555	0.34	25.28 ± 1.06	1.06 ± 0.11	1.57	0.031	2.24	2.12	0.12
	TCTA	555	0.26	32.29 ± 0.57	2.10 ± 0.44	1.20	0.026	2.25	2.07	0.19
2	Zeonex®	521	0.08	8.68 ± 0.09	0.7 ± 0.059	5.16	0.062	2.37	2.26	0.11
	CBP	553	0.29	17.67 ± 0.18	2.7 ± 0.24	1.99	0.033	2.28	2.05	0.22
	TCTA	551	0.14	26.81 ± 0.83	3.92 ± 0.32	1.14	0.037	2.26	2.05	0.21
3	Zeonex®	507	0.06	7.27 ± 0.32	9.90 ± 0.76	3.15	0.061	2.44	2.34	0.10
	CBP	535	0.20	11.84 ± 0.42	10.9 ± 0.66	0.78	0.036	2.33	2.07	0.27
	TCTA	529	0.10	32.45 ± 1.23	5.26 ± 0.71	1.17	0.034	2.34	2.09	0.25

[a] The maximum wavelength of photoluminescence spectra. [b] Photoluminescence quantum yield in degassed. [c] Prompt fluorescence lifetime. [d] Delayed fluorescence lifetime. [e] The ratio of delayed fluorescence (DF) to prompt fluorescence (PF). [f] Activation energy of the triplet to singlet transfer. Error ±0.01 eV. [g] Singlet and triplet energy in. Error ±0.03 eV. [h] Energy splitting. Error ±0.05 eV. All parameters were estimated at 300 K.

benzimidazole)] (50 nm)/LiF (1 nm)/Al (100 nm) (Figure 3). All fabricated devices present a low turn-on voltage between 2.0 V and 3.0 V (Figure 3a). There is significant influence of the donor unit: compounds **1** and **2** formed much more efficient devices than **3** (Figure 3b). The highest external quantum efficiency (EQE) was achieved with device 1, which is fabricated with compound **1** in CBP host (EQE = 9.09%, Figure 3b). Those results are associated with photophysical results, where compound **1** exhibited the highest TADF contribution and photoluminescence quantum yield in comparison to the other compounds. The structural change in the acceptor unit did not affect EQE that much (device 2, Figure 3b) in CBP host. Nevertheless, in TCTA, there is twice decrease in efficiency for more π-conjugated acceptor derivative (compound **2**, devices 4,5) when compared to compound **1**. In contrast, the change in the Si-substituents on the donor connected to acenaphtho[1,2-*b*]pyrido[2,3-*e*]pyrazine acceptor (compound **3**) significantly decreased the EQE (3.68%, Device 3, 6 Figure 3b) in both of the host. The highest luminance was observed in device 4 fabricated with compound **1** in TCTA host, up to 42,000 cd m^{-2} (Figure 3c and d). Change of the acceptor unit in compound **1** (compound **2**) resulted in the decrease of the luminance to 15,000 cd m^{-2} (Device 5, Figure 3c and d), and change of the donor (compound **3**) decreased down to 7,700 cd m^{-2} (device 6, Figure 3c and d).

Theoretical Calculations

Electronic structure calculations allow us to understand further the mechanisms responsible for the observed photophysical behavior. Here we employ density functional theory (DFT) with the long-range corrected functional LC-ωPBE along with the 6-31G(d,p) basis set. The long-range separation parameter of the functional was tuned for all molecules according to the procedure described in reference,[23] and the results are shown in Table S1. Excited state calculations employed the Tamm-Dancoff approximation (TDA),[24] which avoids issues of triplet instability[25] and has been shown to be appropriate for spectrum simulations.[26] Solvent effects were accounted for by means of the polarizable continuum model (PCM)[27] associated with a perturbative state specific solvent approach using parameters for toluene. Finally, spectrum simulations and all rate estimates were calculated using the nuclear ensemble approach as implemented in the NEMO software.[28] A total of 500 geometries were sampled for each case and the QChem 5.0 software[29] was used throughout.

We started our computational analysis by investigating conformational preferences for the three compounds. For this purpose, we performed geometry optimizations at the ground (S_0), S_1 and T_1 states using as initial geometries structures for which the donor and acceptor fragments are orthogonal and parallel to each other. We identified these two arrangements as the equatorial and axial conformations, respectively. Our results show that in the ground state, the equatorial conformation is more stable than the axial one for all compounds (Table S2–S4). However, the energy difference between the two conformers is low, such that the calculation of Boltzmann populations at 300 K indicates that axial conformers are expected to represent 36%, 25% and 38% of the total for compounds **1**, **2**, and **3**, respectively (Table S2–S4). In the excited states, however, the picture is different. As seen in Tables S2–S4, the three compounds show overwhelming preference for the equatorial conformation in the S_1 state, where the donor and the acceptor are almost perpendicular. In the equatorial conformation, the S_1 state displays distinct charge transfer (CT) character from the donor to the acceptor (see NTOs in Figure 4), which is further stabilized under solvation. On the other hand, the T_1 state is more stable in the axial conformation, with the exception of compound **1**, whose T_1 state is energetically lower in the equatorial conformation (Table S2–S4).

Once conformational preferences have been established, we moved on to predicting the photophysics of the three compounds. Fluorescence spectrum simulations can be seen in Figure S7, which show considerable overlap in the spectra of the three compounds. However, peak position shifts from 660 nm for compound **1** to 625 nm for compound **2** and 547 nm for compound **3**. These are qualitatively in good agreement with the experimental results. Estimated fluorescence rates are rather low, ranging from 1.4×10^6 s^{-1} for compound **3** to 4.6×10^6 s^{-1} for compound **2** (detailed values and error estimates can be found in Table S5). These low values result from the strong CT character of their S_1 states, as transitions from CT states are known to display low oscillator strengths. Yet, these fluorescence rates still outcompete the phosphorescence rates from the triplet excited states, T_1 and T_2 (Table S6), which is in good agreement with the fact that only TADF was observed in matrices (Figure 2).

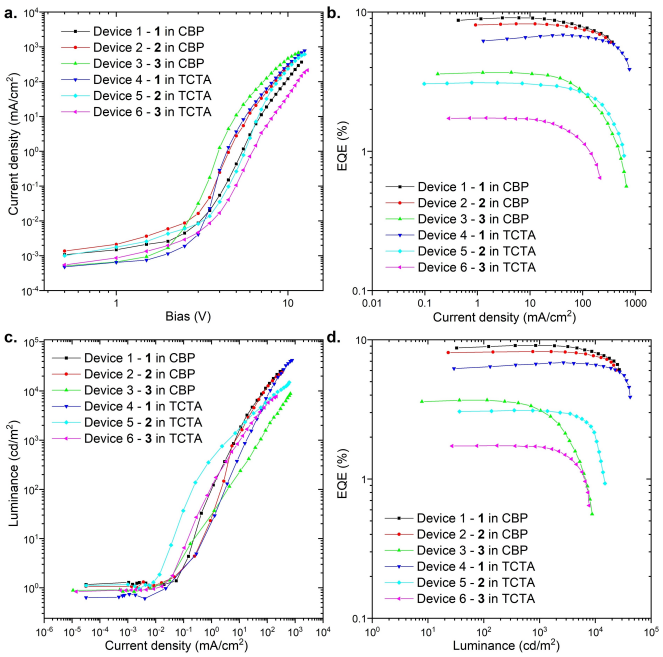

Figure 3. The characteristics of the OLED devices. a) Current density-bias characteristics. b) EQE-current density characteristics. c) Luminance-current density characteristics. d) EQE-luminance characteristics.

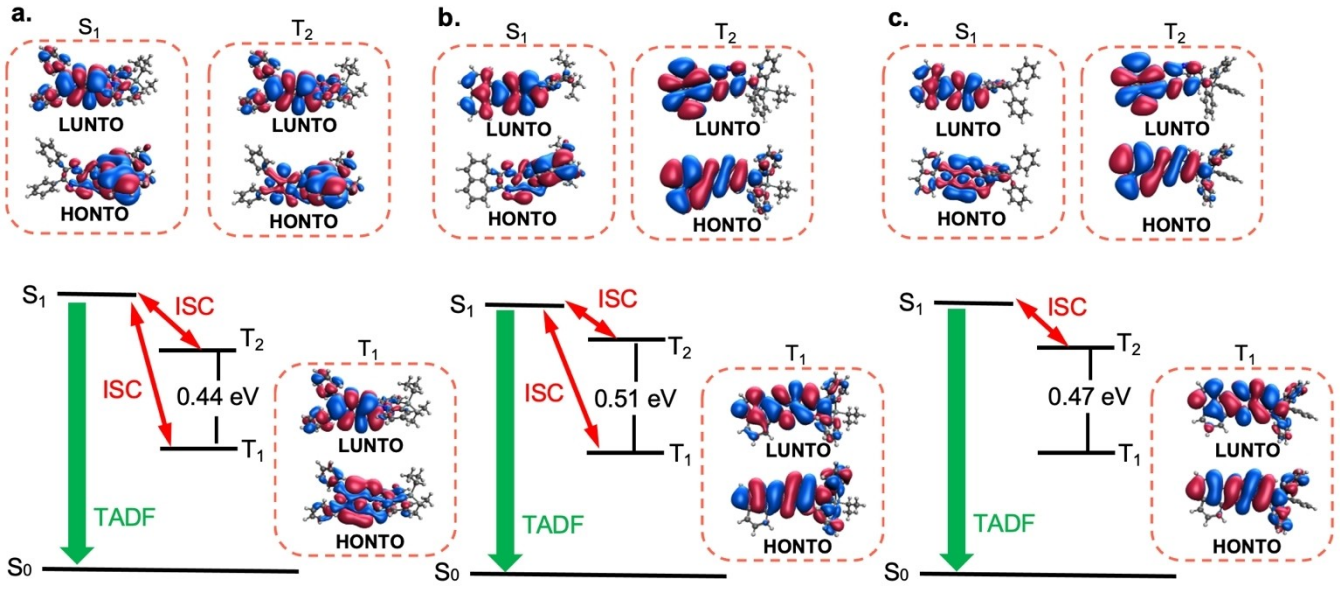

Figure 4. Natural Transition Orbitals (NTOs) for the S_1, T_1 and T_2 states for a) **1**, b) **2**, and c) **3**. The diagrams indicate the processes expected to take place for each molecule as predicted by the theoretical calculations.

To determine the dynamics of excited states in these compounds, in addition to estimating fluorescence rates, we calculated intersystem crossing (ISC) rates using S_1 as the initial state. These estimates are shown in Table S7, and the data revealed that, for all the compounds, ISC rates can be significantly higher than fluorescence rates. By calculating the ratio between the rates of each process and the sum of ISC and fluorescence rates, we may estimate the probability of each individual process taking place. For compounds **1** and **2**, the highest probabilities are associated with ISC transfers from S_1 to T_1 and T_2, with T_2 being the most probable one. For compound **3**, however, ISC rates from S_1 to T_1 are much lower than that for T_2, which is by far the preferred outcome. Prompt emission in the three compounds, in contrast, is expected in less than 1% of cases as a result of the weakly allowed S_1 CT transitions. Given the significant TADF emission in matrices, the triplet recycling through ISC and rISC is very efficient for these molecules.

ISC transfers to triplet states above T_2 also display significant probability (ranging from 10% to 20%, Figure S9). As such, it is worth looking into the energy gaps between the different triplet states, as internal conversion between these states is expected to be the preferred mechanism of relaxation. Table S10 shows the average gap between triplet states calculated from the 500 geometries sampled for use by the nuclear ensemble method. It can be seen that the average gaps between triplet states above T_2 are between 0.2 and 0.3 eV. In contrast, T_2-T_1 gaps range from 0.4 to 0.5 eV. These results suggest that molecules that undergo ISC to T_3 or higher triplets are likely to suffer internal conversion back to the T_2 state, whereas the high T_2-T_1 gap may prevent efficient internal conversion back to T_1. This means that it is necessary to analyze ISC and phosphorescence rates from both T_1 and T_2 states.

The estimation of rates for reverse ISC (rISC) from the T_1 state to S_n states are shown in Tables S8. We focused on compounds **1** and **2**, that as mentioned above, are expected to have the T_1 state populated by means of ISC from S_1. Comparing these two molecules, we observed that compound **1** shows orders of magnitude higher rISC (Table S8) than compound **2**. This difference can be attributed to the fact that the T_1 state is more stable in the equatorial conformation for compound **1**, whereas it is more stable in the axial conformation for compound **2**. One key difference between these two conformations that accounts for the difference in rates is that reorganization energies for T_1 to S_1 transfers in the axial conformation are much higher (~0.50 eV) than in the equatorial one (~0.25 eV). On the other hand, phosphorescence energies for the three compounds do not differ so significantly (ranging from 670 nm to 725 nm) and the T_1 phosphorescence spectra (shown in Figure S8) show strong overlap. In addition to the difference in rates, T_1 states in compounds **1** and **2** have different expected behaviors as well. In the case of compound **1**, rISC transfers to S_1 dominate, whereas for compound **2** there is an almost even split between phosphorescence and rISC. However, since the rates in question are very low, the T_1 states in compound **2** are good candidates for non-radiative deexcitation.

Finally, we turned to the estimation of rISC rates from the T_2 state. These can be seen in Tables S9. The rISC rates from T_2 to S_n states are larger than those from T_1 for all three compounds, but the rISC rates from T_2 to S_1 are much larger than other transitions and are expected to be the dominant mechanism of T_2 depopulation followed by TADF pathway. As such, following the previous discussion, we expect a continuous interconversion between S_1 and T_2 states (also T_1 in the case of compounds **1** and **2**) followed by delayed emission (TADF) from the S_1 state (Figure 4). The low fluorescence rates combined with this

continuous interconversion of triplets and singlets also provide many opportunities for non-radiative decay other than TADF channel, from which we expect to observe low luminescence quantum yields for all three compounds. This would be the reason why these molecules show moderate TADF efficiency. In terms of emission wavelength, T_2 phosphorescence spectrum simulations (shown in Figure S9) differ significantly among the three compounds, with emission peaks being evaluated at 548 nm, 484 nm and 596 nm for compounds **1**, **2** and **3**, respectively.

Figure 4 summarizes the calculation results discussed above by showing the most relevant mechanisms expected to take place for each of the 3 compounds, namely ISC from S_1 to T_1 and T_2 followed by rISC back to S_1 from where delayed emission is observed. For compound **3**, a similar mechanism is presented, with the exception that ISC from S_1 to T_1 is expected to be much less efficient than ISC from S_1 to T_2. As such, only rISC from T_2 collaborates to the repopulation of singlet states and the consequent delayed emission.

Conclusion

In summary, we have successfully developed a new family of TADF emitters, utilizing the D–A scaffold comprising of polyazaaromatics, i.e., pyrido[2,3-*b*]pyrazines, and dihydrophenazasilines as the donor. The time-resolve spectroscopic analysis revealed that these compounds show TADF in matrices. Furthermore, the OLEDs fabricated with developed D–A molecules achieved a high external quantum efficiency (EQE) up to 9%, exceeding the theoretical maximum of those fabricated with prompt fluorescence emitters (5%). Furthermore, theoretical calculations revealed the importance of the high triplet excited state (T_2) as the intermediate of efficient rISC process to yield TADF within the D–A scaffold.

Acknowledgements

*Y.T. acknowledges a Grant-in-Aid for Scientific Research on Innovative Area "Aquatic Functional Materials: Creation of New Materials Science for Environment-Friendly and Active Functions" (JSPS KAKENHI Grant Number JP19H05716) from the MEXT (Ministry of Education, Culture, Science and Technology, Japan), a Grant-in-Aid for Scientific Research (B) (JSPS KAKENHI Grant Number JP20H02813), a Grant-in-Aid for Challenging Research (Exploratory) (JSPS KAKENHI Grant Number JP21K18960), and the Continuation Grants for Young Researchers from the Asahi Glass Foundation, and the Research Grant in the Natural Science from the Mitsubishi Foundation. Y.T. and S.M. acknowledge NIPPOH CHEMICALS for supplying N,N-*diiodo-5,5-dimethylhydantoin (DIH). P. de S. and L. E. de S. acknowledge support by a research grant (00028053) from VILLUM FONDEN. P.D. and P.Z.C acknowledges the Polish National Science Centre funding, grant no. 2017/25/B/ST5/02488. P.D. and P.Z.C acknowledges the supporting awards from the Rector of the Silesian University of Technology (04_040_SDU_10-22-04, 04/040/RGJ21/0149). Y.T., P.Z.C., P. de S. and P.D. acknowledge the EU's Horizon 2020 for funding the OCTA project under grant agreement No 778158. Research work supported from the funds for science in 2018–2022 allocated to the implementation of an international co-financed project by the Polish Ministry of Education and Science. P.D. and P.Z.C. acknowledges the supporting actions from EU's Horizon 2020 ERA-Chair project ExCEED, grant agreement No 952008.*

Conflict of Interest

The authors declare no conflict of interest.

Data Availability Statement

The data that support the findings of this study are available in the supplementary material of this article.

Keywords: thermally activated delayed fluorescence · donor-acceptor · charge-transfer · OLED · azaheterocycle

[1] H. Uoyama, K. Goushi, K. Shizu, H. Nomura, C. Adachi, *Nature* **2012**, *492*, 234–238.
[2] a) Y. Tao, K. Yuan, T. Chen, P. Xu, H. Li, R. Chen, C. Zheng, L. Zhang, W. Huang, *Adv. Mater.* **2014**, *26*, 7931–7958; b) Z. Yang, Z. Mao, Z. Xie, Y. Zhang, S. Liu, J. Zhao, J. Xu, Z. Chi, M. P. Aldred, *Chem. Soc. Rev.* **2017**, *46*, 915–1016; c) F. B. Dias, T. J. Penfold, A. P. Monkman, *Methods Appl. Fluoresc.* **2017**, *5*, 012001; d) Y. Im, M. Kim, Y. J. Cho, J.-A. Seo, K. S. Yook, J. Y. Lee, *Chem. Mater.* **2017**, *29*, 1946–1963; e) Y. Liu, C. Li, Z. Ren, S. Yan, M. R. Bryce, *Nat. Rev. Mater.* **2018**, *3*, 1–20; f) T. Huang, W. Jiang, L. Duan, *J. Mater. Chem. C* **2018**, *6*, 5577–5596; g) M. Godumala, S. Choi, M. J. Cho, D. H. Choi, *J. Mater. Chem.* **2019**, *7*, 2172–2198; h) X. Liang, Z.-L. Tu, Y.-X. Zheng, *Chem. Eur. J.* **2019**, *25*, 5623–5642; i) P. Data, Y. Takeda, *Chem. Asian J.* **2019**, *14*, 1613–1636; j) H. Nakanotani, Y. Tsuchiya, C. Adachi, *Chem. Lett.* **2021**, *50*, 938–948.
[3] X. Xiong, F. Song, J. Wang, Y. Zhang, Y. Xue, L. Sun, N. Jiang, P. Gao, L. Tian, X. Peng, *J. Am. Chem. Soc.* **2014**, *136*, 9590–9597.
[4] T. Li, D. Yang, L. Zhai, S. Wang, B. Zhao, N. Fu, L. Wang, Y. Tao, W. Huang, *Adv. Sci.* **2017**, *4*, 1600166.
[5] V.-N. Nguyen, A. Kumar, M. H. Lee, J. Yoon, *Coord. Chem. Rev.* **2020**, *425*, 213545.
[6] L. Candish, K. D. Collins, G. C. Cook, J. J. Douglas, A. Gómez-Suárez, A. Jolit, S. Keess, *Chem. Rev.* **2021**, DOI 10.1021/acs.chemrev.1c00416.
[7] Y. Takeda, P. Data, S. Minakata, *Chem. Commun.* **2020**, *56*, 8884–8894.
[8] P. Data, P. Pander, M. Okazaki, Y. Takeda, S. Minakata, A. P. Monkman, *Angew. Chem. Int. Ed.* **2016**, *55*, 5739–5744; *Angew. Chem.* **2016**, *128*, 5833–5838.
[9] a) S. Izumi, H. F. Higginbotham, A. Nyga, P. Stachelek, N. Tohnai, P. de Silva, P. Data, Y. Takeda, S. Minakata, *J. Am. Chem. Soc.* **2020**, *142*, 1482–1491; b) A. Nyga, S. Izumi, H. F. Higginbotham, P. Stachelek, S. Pluczyk, P. Silva, S. Minakata, Y. Takeda, P. Data, *Asian J. Org. Chem.* **2020**, *9*, 2153–2161.
[10] a) H. F. Higginbotham, M. Okazaki, P. de Silva, S. Minakata, Y. Takeda, P. Data, *ACS Appl. Mater. Interfaces* **2021**, *13*, 2899–2907; b) T. Hosono, N. O. Decarli, T. Goya, L. E. de Sousa, N. Tohnai, S. Minakata, P. de Silva, P. Data, Y. Takeda, *J. Mater. Chem. C* **2021**, DOI: 10.1039/d1tc05730h.
[11] M. Okazaki, Y. Takeda, P. Data, P. Pander, H. Higginbotham, A. P. Monkman, S. Minakata, *Chem. Sci.* **2017**, *8*, 2677–2686.
[12] Y. Takeda, T. Kaihara, M. Okazaki, H. Higginbotham, P. Data, N. Tohnai, S. Minakata, *Chem. Commun.* **2018**, *54*, 6847–6850.
[13] H. Yamagishi, S. Nakajima, J. Yoo, M. Okazaki, Y. Takeda, S. Minakata, K. Albrecht, K. Yamamoto, I. Badía-Domínguez, M. M. Oliva, M. C. R. Delgado, Y. Ikemoto, H. Sato, K. Imoto, K. Nakagawa, H. Tokoro, S.-I. Ohkoshi, Y. Yamamoto, *Commun. Chem.* **2020**, *3*, 1–8.

[14] S. Yamauchi, N. Hirota, *J. Phys. Chem.* **1987**, *91*, 1754–1760.
[15] M. A. El-Sayed, *Acc. Chem. Res.* **1968**, *1*, 8–16.
[16] T. Huang, D. Liu, J. Jiang, W. Jiang, *Chem. Eur. J.* **2019**, *25*, 10926–10937.
[17] W. Yang, Y. Yang, L. Zhan, K. Zheng, Z. Chen, X. Zeng, S. Gong, C. Yang, *Chem. Eng. J.* **2020**, *390*, 124626.
[18] L. Yu, Z. Wu, G. Xie, J. Luo, Y. Zou, D. Ma, C. Yang, *J. Mater. Chem. C* **2020**, *8*, 12445–12449.
[19] Q. Peng, L. Yang, Y. Li, Y. Zhang, T. Li, Y. Qin, Y. Song, H. Hou, K. Li, *J. Phys. Chem. C* **2020**, *124*, 22684–22691.
[20] S. S. Mahadik, D. R. Garud, A. P. Ware, S. S. Pingale, R. M. Kamble, *Dyes Pigm.* **2021**, *184*, 108742.
[21] L. Yin, J. Liebscher, *Synthesis* **2005**, *2005*, 1345–1349.
[22] G. Kaur, A. Singh, N. Kaur, B. Banerjee, *Synth. Commun.* **2021**, *51*, 1121–1131.
[23] T. Stein, L. Kronik, R. Baer, *J. Am. Chem. Soc.* **2009**, *131*, 2818–2820.
[24] S. Hirata, M. Head-Gordon, *Chem. Phys. Lett.* **1999**, *314*, 291–299.
[25] M. J. G. Peach, M. J. Williamson, D. J. Tozer, *J. Chem. Theory Comput.* **2011**, *7*, 3578–3585.
[26] A. Chantzis, A. D. Laurent, C. Adamo, D. Jacquemin, *J. Chem. Theory Comput.* **2013**, *9*, 4517–4525.
[27] G. Scalmani, M. J. Frisch, *J. Chem. Phys.* **2010**, *132*, 114110.
[28] a) L. E. de Sousa, P. de Silva, *J. Chem. Theory Comput.* **2021**, *17*, 5816–5824; b) https://github.com/LeonardoESousa/NEMO.
[29] Y. Shao, Z. Gan, E. Epifanovsky, A. T. B. Gilbert, M. Wormit, J. Kussmann, et al. *Mol. Phys.* **2015**, *113*, 184–215.

Manuscript received: December 16, 2021
Revised manuscript received: January 23, 2022
Accepted manuscript online: January 25, 2022
Version of record online: February 19, 2022